Evaluation of the upconversion mechanisms in Ho^{3+}-doped crystals: Experiment and theoretical modeling

E. Osiac,[1,2,*] I. Sokólska,[1,3] and S. Kück[1]
[1]*Institut für Laser-Physik, Jungiusstraße 9a, 20355 Hamburg, Germany*
[2]*Institute of Atomic Physics, P.O. Box: MG-6, 76900 Bucharest, Romania*
[3]*Institute of Low Temperature and Structure Research, Polish Academy of Sciences, 50-950 Wrocław, Poland*
(Received 19 November 2001; revised manuscript received 22 January 2002; published 14 June 2002)

The paper compares the mechanisms that enable the upconverted green emission ($^5S_2 \rightarrow {}^5I_8$) of the Ho^{3+} ion under infrared excitation (700–920 nm) in several crystalline hosts ($YAlO_3$, $YLiF_4$, $Y_3Sc_2Ga_3O_{12}$, and BaY_2F_8). Parameters involved in the upconversion such as excited-state absorption and cross-relaxation rates were determined from spectroscopic measurements. A system of differential equation (rate equations) was used to describe the upconversion mechanism and was numerically solved. The results were compared with experimental data. A reduction of this system to a three-level ''simplified system'' is presented, which includes only the ground level, the emitting level, and the intermediate level. The differences between the photon-avalanche mechanism and the looping mechanism are discussed and analyzed according to this simplified system.

DOI: 10.1103/PhysRevB.65.235119 PACS number(s): 78.20.Bh

I. INTRODUCTION

Ho^{3+} is a very interesting ion from the point of view of upconversion, cross-relaxation, and excited-state absorption (ESA) processes. Its energy-level scheme (Fig. 1) allows multiple ESA transitions from the $^5I_7$, $^5I_6$, and $^5I_5$ levels to the $^5S_2$ or higher-lying levels, which could activate emission from these high-lying levels and make these systems interesting for upconversion lasers.

Green emission based on an avalanche-type mechanism was obtained in Ho^{3+}:$YAlO_3$ and Ho^{3+}:ZBLAN under a 580-nm pump.[1,2] In our study we will focus on the range of infrared excitation (700–920 nm), where efficient laser diodes are available. Under excitation in this spectral range, strong green emission ($^5S_2 \rightarrow {}^5I_8$) was reported in several crystals.[1,3–5]

The excitation spectrum in this region reveals that the $^5S_2$ multiplet is excited after pumping around 750, 840, and 890 nm (from which excitation around 840 nm leads to the weakest green emission). The comparison with the absorption spectra leads to the assumption that the mechanisms under 750- and 840-nm excitation are mainly due to strong ESA processes, while the 890-nm excitation mechanism is more likely a two-step absorption. Excitation mechanisms were previously presented and discussed for $YAlO_3$ (Refs. 1 and 4) and $YLiF_4$ (YLF) (Ref. 3) under a 750-nm pump and BaY_2F_8 (BYF) (Ref. 5) under a 888-nm pump. A short description of these mechanisms in the beginning will be helpful in understanding our further analysis.

For crystals with relative high phonon energy, such as $YAlO_3$ (effective phonon energy $\hbar\omega \sim 600\ cm^{-1}$), YLF ($\hbar\omega \sim 490\ cm^{-1}$), and $Y_3Sc_2Ga_3O_{12}$ (YSGG) ($\hbar\omega \sim 550\ cm^{-1}$) the case of 750-nm excitation was found to be the most favorable in order to obtain green emission. In this case, a very weak ground-state absorption [$^5I_8 \rightarrow {}^5I_4$, GSA1 in Fig. 1(a)] triggers the process. Phonon deexcitation $^5I_4 \rightarrow {}^5I_5 \rightarrow {}^5I_6 \rightarrow {}^5I_7$ brings the excitation to the $^5I_7$. A strong ESA process [$^5I_7 \rightarrow {}^5S_2$, ESA1 in Fig. 1(a)] enables the population of the $^5S_2$ multiplet. The cross-relaxation process s [($^5S_2$, $^5I_8$)$\rightarrow$($^5I_4$, $^5I_7$)] creates the possibility for further feeding the $^5I_7$ multiplet. Additionally a second ESA process [$^5I_6 \rightarrow {}^5G_6$, ESA2 in Fig. 1(a)] occurs. Nevertheless, although this excitation scheme works for both Ho^{3+}:$YAlO_3$ and Ho^{3+}:YLF, a different behavior for the upconverted green emission was reported for YLF (Ref. 4) and $YAlO_3$.[5] For the green emission of Ho^{3+}:YLF, features of an avalanche mechanism were observed, while the upconverted green emission in the case of $YAlO_3$ shows none of the avalanche characteristics. In this latter case (Ho^{3+}:$YAlO_3$), a so-called ''looping mechanism'' (Ref. 6) is being established. The name is due to the fact that when an excited ion is removed from the $^5I_7$ level by the ESA1 process $^5I_7 \rightarrow {}^5S_2$ it will enable processes which again populate the $^5I_7$ level (cross-relaxation s and phonon deexcitation chain $^5I_4 \rightarrow {}^5I_5 \rightarrow {}^5I_6 \rightarrow {}^5I_7$). This behavior is similar to a loop, i.e., a round trip of the excitation in the system. It should be mentioned that the cross-relaxation process s not only creates a loop in the excitation circuit but also brings new excitation into it (due to the component $^5I_8 \rightarrow {}^5I_7$). In this way any loop also creates a gain in the excitation of the intermediate level. The ratios between the gain of the excitation loop and the loss in the population of the $^5I_7$ level plays a major role in the behavior of the system. In one part of this paper this different behavior for the cases of Ho^{3+}:$YAlO_3$ and Ho^{3+}:YLF under 750-nm excitation will be presented and analyzed in terms of this gain and loss. This is a similar treatment to the one presented in Ref. 6 for Ho^{3+}, Tm^{3+}:$Gd_3Ga_5O_{12}$. This means the introduction of a new ''simplified system'' of equations, where only the ground state, the intermediate level for the looping mechanism, and the emitting level will be considered.

In the case of Ho^{3+}:BYF ($\hbar\omega \sim 360–380\ cm^{-1}$) under 750-nm excitation the $^5I_6$ multiplet acts like a trap for the excitation (due to low multiphonon deexcitation rates) and makes the feeding process of the $^5I_7$ level inefficient. The

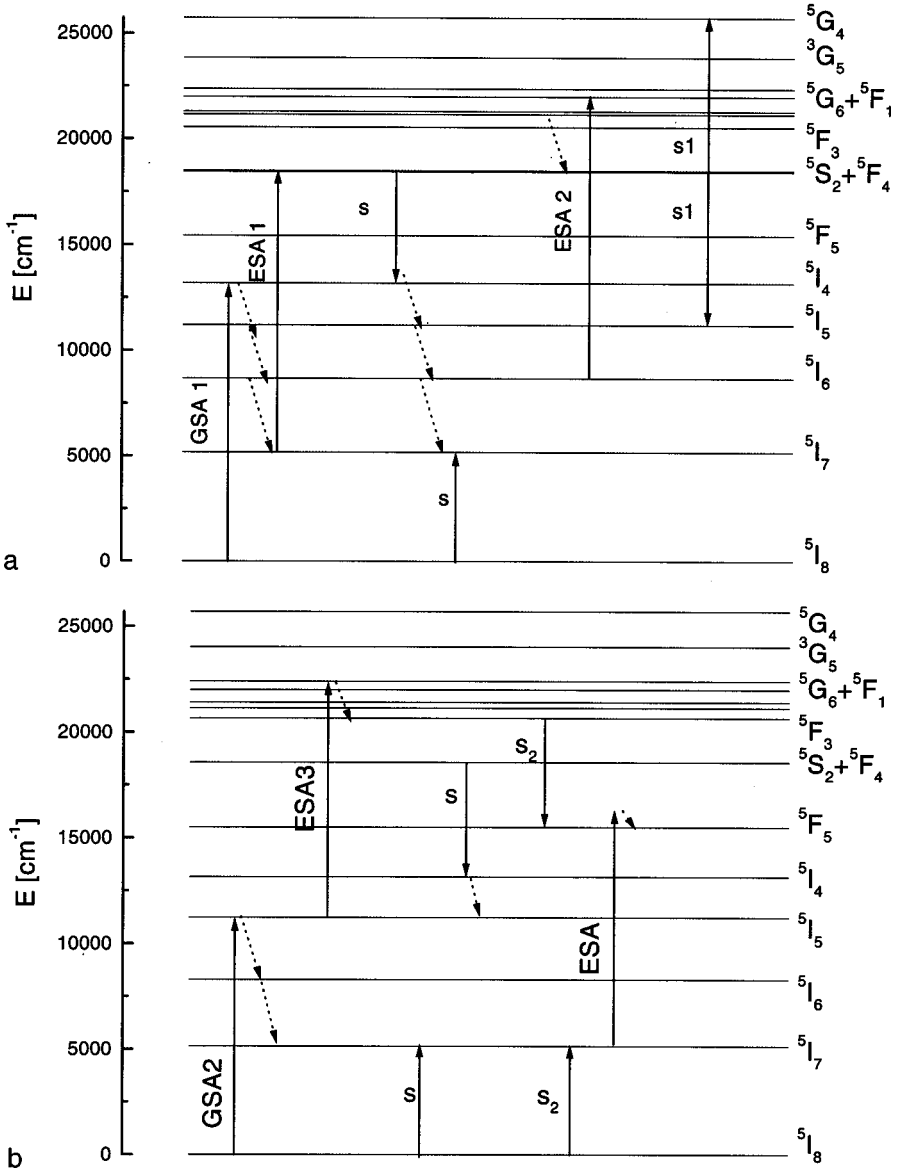

FIG. 1. (a) Upconversion scheme for 750-nm excitation (e.g., Ho^{3+}:YLF). (b) Upconversion scheme for 888-nm excitation (e.g., Ho^{3+}:BYF).

second ESA process ($^5I_6 \rightarrow {}^5G_6$) brings the excitation to levels higher than the $^5S_2$ level. Parts of this excitation bypass the $^5S_2$ level, because these levels are not totally quenched by phonon deexcitation and due to cross-relaxation processes such as, e.g., ($^5F_3$, $^5I_8$)$\rightarrow$($^5F_5$, $^5I_7$). The gain of this excitation loop is thus very small. For Ho^{3+}:BYF another upconversion scheme, leading to the most intense green upconverted emission was proposed [see Fig. 1(b)]. This mechanism is based on a two-step absorption process under 890-nm excitation: ground-state absorption $^5I_8 \rightarrow {}^5I_5$ followed by the ESA $^5I_5 \rightarrow {}^5F_1$. Several cross-relaxation processes [i.e., s ($^5S_2$, $^5I_8$)$\rightarrow$($^5I_4$, $^5I_7$) and s_2 ($^5F_3$, $^5I_8$) $\rightarrow$($^5F_5$, $^5I_7$)] also act in the system, but they do not provide additional excitation to the intermediate level ($^5I_5$). A second, but very weak ESA process ($^5I_7 \rightarrow {}^5F_5$) also exists in this scheme. In this paper we will extend these analyses, providing a comparative investigation of the ESA processes together with numerical simulations and analytical calculations.

II. EXPERIMENT

Ho^{3+}:$YAlO_3$ and Ho^{3+}:YLF crystals doped with 0.1%, 1% and 3%, and Ho^{3+}:BYF and Ho^{3+}:YSGG crystals doped with 1% of Ho^{3+} ions were grown by the Czochralski method. All concentrations are given with respect to the Y site. All measurements were performed at room temperature. For the absorption spectra a Cary 2400 spectrophotometer was used. For the emission spectra the samples were excited by a continuous-wave Ti:sapphire laser (Spectra-Physics 3900S) pumped by a frequency-doubled Nd:YVO_4 (Spectra-Physics Millennia X), and the signal was collected (under 90°) by a cooled S1 photomultiplier placed behind a 0.5-m Spex monochromator. The wavelength of the monochromator is computer controlled. The excitation measurements were performed in the same setup as the emission measurements, but in these cases the wavelength of the Ti:sapphire laser was scanned while the wavelength of the monochromator was fixed. The wavelength scan of the Ti:sapphire laser was performed using a birefringent filter in the laser

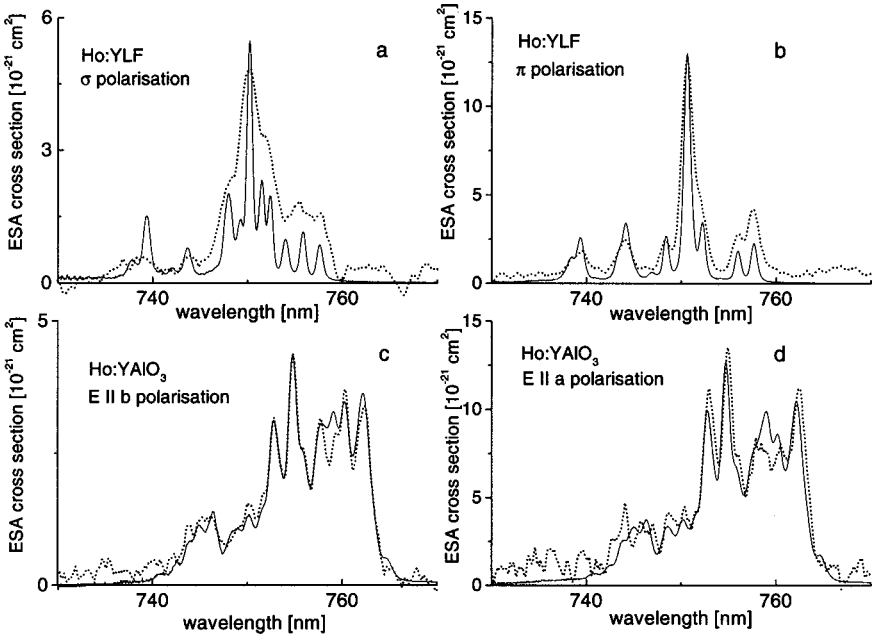

FIG. 2. Excited-state absorption spectra measured (dotted line) and calculated by the reciprocity method (solid line) for Ho^{3+}:YLF [(a) and (b)] and Ho^{3+}:$YAlO_3$ [(c) and (d)] at RT.

cavity in connection with a computer-controlled stepper motor. For the kinetics measurements (i.e., decays and temporal evolutions of populations) an oscilloscope (LeCroy 9060) was used.

The ESA measurements were performed in accordance with the setup described in detail in Ref. 7. This method is a pump-and-probe measurement using a double modulation technique with two lock-in amplifiers. The probe beam is provided by a halogen lamp, and is modulated by a light chopper with a frequency of about 800 kHz. The transmitted signal is analyzed with the first look-in amplifier, which uses this high-frequency chopper as reference. The pump beam is provided by a laser, and is modulated with a much lower frequency of about 10 Hz. Its aim is to bring a number of ions into the excited states, and consequently the probe beam absorption does not only occur from the ground state but also from the excited states. Furthermore, amplification of the probe beam due to stimulated emission will be measured. Because the second look-in amplifier uses the output signal of the first lock-in amplifier as an input signal and operates with the reference signal from the pump beam (10 Hz), it will analyze the difference between the transmission signal in the presence (I_p) or absence (I_u) of excitation due to the pump beam. It should be mentioned that an almost perfect overlap between the path of the probe beam and the path of the pump beam inside the crystal should be realised in the experiment.

It can be shown that the following formula holds:

$$\Delta I/I = A^* \left[\sigma_{\mathrm{GSA}} + \sum_i (n_i/n_e)(\sigma_{\mathrm{em},i} - \sigma_{\mathrm{ESA},i}) \right] \qquad (1)$$

where ΔI is the difference between the transmission signal in the presence (I_p) or absence (I_u) of the pump laser signal applied; I is the transmitted signal ($I \approx I_p \approx I_u$); σ_{GSA}, $\sigma_{\mathrm{em},i}$, and $\sigma_{\mathrm{ESA},i}$ are the ground-state absorption cross section, the emission cross section for the level i, and the excited-state absorption cross section for the level i, respectively; n_i is the population of the ith excited state; $n_e = \Sigma_i n_i$ is the total population of the excited states; and A is a constant. To obtain this formula the assumption was made that the difference ΔI is small in order to approximate the expression $\ln(1+\Delta I/I_u)$ with $\Delta I/I_u$. This approximation holds when the number of excited ions is small compared with the total number of ions (small pump power densities). The signal $\Delta I/I$ is positive in the case of dominating ground-state absorption or stimulated emission and negative in the case of dominating excited state absorption.

One of the main tasks was to determine the ESA cross sections for the $^5I_7 \rightarrow {}^5S_2$ and $^5I_6 \rightarrow {}^5G_6$ transitions. With the help of the above method we measured the $\Delta I/I$ signal in the spectral range of 730–770 nm in order to determine the cross section for the $^5I_7 \rightarrow {}^5S_2$ transition. In Figs. 2(a)–2(d) the results (dotted line) for the case of Ho^{3+}:YLF and Ho^{3+}:$YAlO_3$ are presented. Using the above-described method, the results are obtained in arbitrary units. They were normalized to cross-section values with a procedure, which is based on the reciprocity method and will be described in the following. For the case of Ho^{3+}:BYF the $\Delta I/I$ signal is presented for the range of 700–900 nm in Fig. 3(a) and in detail for the 880–900-nm region in Fig. 3(b) (corresponding to the $^5I_8 \rightarrow {}^5I_5$ and $^5I_5 \rightarrow {}^5F_1$ transitions).

The ESA signal ($^5I_7 \rightarrow {}^5S_2$) can also be estimated using the reciprocity method [Eq. (2)], if the emission cross section is known. The emission cross section ($^5S_2 \rightarrow {}^5I_7$) can be calculated using the Fuechtbauer-Ladenburg formula [Eq. (3)]

$$\sigma_{\mathrm{em}}(\lambda) = \sigma_{\mathrm{abs}}(\lambda) \frac{Z_L}{Z_U} \exp\left(E_{ZL} - \frac{hc}{\lambda} \right), \qquad (2)$$

$$\sigma_{\mathrm{em}}(\lambda) = C\lambda^5 I(\lambda), \qquad (3)$$

where σ_{em} and σ_{abs} are the emission and absorption cross sections, Z_L and Z_U are the partition function for the lower

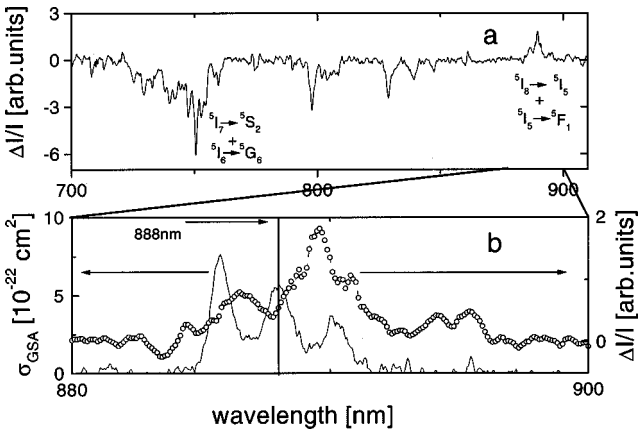

FIG. 3. (a) Measured $\Delta I/I$ spectrum between 700 and 910 nm. (b) Ground-state absorption (solid line) and measured $\Delta I/I$ spectrum (open circles) around 890 nm for Ho^{3+}:BYF at RT.

and upper multiplets, E_{ZL} is the energy of the transition between the lowest levels of the upper and lower multiplets (the so called zero-line energy), $I(\lambda)$ is the spectral intensity distribution (photons/s), and C is a constant. In order to calculate Z_L and Z_U we used the energy-level data reported in Refs. 8–10 for Ho^{3+}:YLF, in Ref. 1 for Ho^{3+}:$YAlO_3$, and in Refs. 11 and 12 for Ho^{3+}:YSGG. The values are listed in Table I.

In our case (Ho^{3+}:YLF and Ho^{3+}:$YAlO_3$ and the $^5I_7 \rightarrow {}^5S_2$ transition as the ESA process), the ground-state absorption cross section ($^5I_8 \rightarrow {}^5S_2$) was first measured. By the reciprocity method the emission cross section ($^5S_2 \rightarrow {}^5I_8$) was determined. By using Eq. (3) it was then possible to determine the $^5S_2 \rightarrow {}^5I_7$ emission cross section.

The results of the $^5I_7 \rightarrow {}^5S_2$ absorption from the direct ESA measurements (dotted lines) and from the $^5S_2 \rightarrow {}^5I_7$ emission spectra via the reciprocity method (solid lines) are presented in Figs. 2(a) and 2(b) for Ho^{3+}:YLF (σ and π polarizations), and in Figs. 2(c) and 2(d) for Ho^{3+}:$YAlO_3$ (a and b polarizations).

In the case of Ho^{3+}:BYF the $\Delta I/I$ spectrum is presented in Fig. 3(a). It is observed, that a pure ESA signal exists in the spectral ranges around 750, 800, and 840 nm. In the 888-nm range the signal is positive, but if we compare it with the ground-state absorption spectrum [see Fig. 3(b)], it can be observed that the $\Delta I/I$ signal is almost zero at 888 nm although the ground-state absorption cross section spectra has a maximum at 888 nm. This proves that at this wavelength a strong ESA transition also exists.

The excitation spectra of the green emission are presented in Figs. 4(a)–4(d). For Ho^{3+}:BYF the excitation spectra is compared with the ground-state absorption spectra [see Fig. 4(a)] around 890 nm. In the case of Ho^{3+}:YLF the excitation and the ESA spectrum of the $^5I_7 \rightarrow {}^5S_2$ transition are presented in Fig. 4(b). For the case of Ho^{3+}:$YAlO_3$ and Ho^{3+}:YSGG the excitation spectra are also presented in Figs. 4(c) and 4(d) in comparison with the corresponding ESA spectra.

The parameters necessary for the numerical simulations were obtained by analyses of the kinetics measurements. Transfer rates were calculated from the decay curves by using the formula

$$W_t = W_{EF} - W_0, \tag{4a}$$

where W_0 is the deexcitation rate in the absence of transfer and W_{EF} is the rate in the presence of energy transfer and could be estimated from Eq. (4b),[13]

$$W_{EF} = \frac{1}{\int_0^\infty n(t)dt}, \tag{4b}$$

where $n(t)$ represents the decay curve, normalized to the maximal value.

In order to calculate these rates the decays for samples with a low Ho^{3+} concentration (0.1%) were measured. At low dopant concentration there is almost no energy transfer between the dopant ions, and consequently the decay is exponential and the lifetime τ_0 can be easily obtained by a fit. The deexcitation rate will be $W_0 = 1/\tau_0$. Increasing the concentration of the dopant ion the non-radiative energy transfer between the dopant ions starts to play an important role. The decays become non-exponential, so the fit with an exponential function gives not accurate values for the lifetimes. In fact one can define only a mean lifetime[13] and an effective dexcitation rate as given by Eq. (4b). According to Eq. (4a) the difference between these two rates will give us a value for the transfer rates. In fact, these values will represent a mean value of the individual transfer rates from each pair of dopant ions, but it will be appropriate to be used into a rate equation model.

Additionally, the quantum yield of the transfer process can be derived from Eq. (5),[13]

$$\eta = 1 - \frac{1}{\tau_0}\int_0^\infty n(t)dt = 1 - \frac{W_0}{W_{EF}} = \frac{W_t}{W_{EF}}, \tag{5}$$

TABLE I. The partition function Z for $^5I_8$, $^5I_7$, and ($^5S_2$, $^5F_4$) multiplets.

System	$Z(^5I_8)$	$Z(^5I_7)$	$Z(^5S_2+{}^5F_4)$
Ho^{3+}:YLF	6.91	8.59	6.67
(Refs. 8–10)	(13 Stark level reported)	(10 Stark level reported)	(4+7 Stark level reported)
Ho^{3+}:$YAlO_3$	7.6	6.86	9.28
(Ref. 1)	(16 Stark level reported)	(11 Stark level reported)	(5+9 Stark level reported)
Ho^{3+}:YSGG	6.97	8.89	6.99
(Refs. 11 and 12)	(14 Stark level reported)	(13 Stark level reported)	(5+8 Stark level reported)

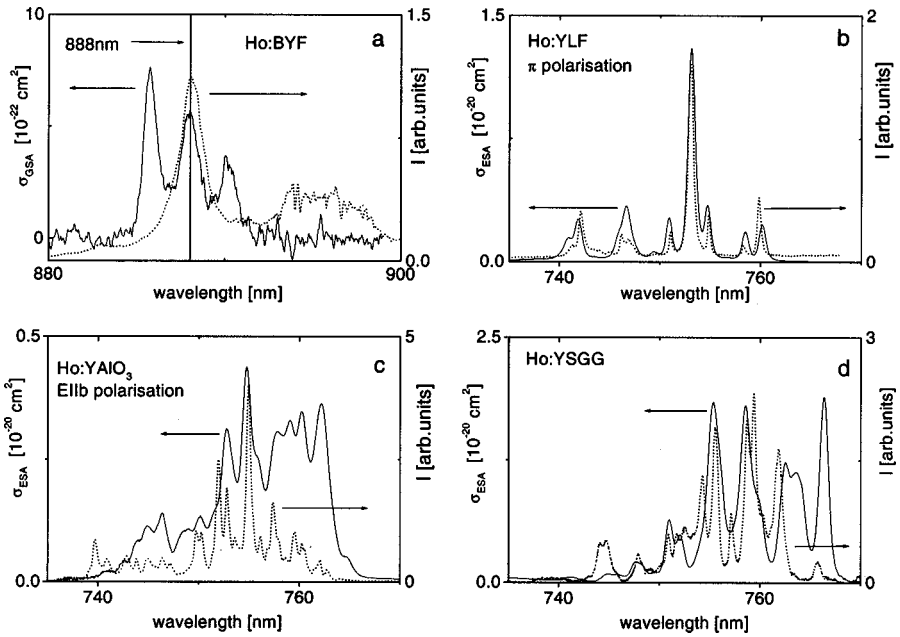

FIG. 4. Excitation spectra (for green emission $^5S_2 \rightarrow {}^5I_8$) (dotted line) for Ho^{3+}:BYF (a), Ho^{3+}:YLF (b), Ho^{3+}:$YAlO_3$ (c), and Ho^{3+}:YSGG (d), ESA spectra (solid) line) for Ho^{3+}:YLF (b), Ho^{3+}:$YAlO_3$ (c), and Ho^{3+}:YSGG (d) and GSA spectra (solid line) for Ho^{3+}:BYF (a), at RT.

where $\tau_0 = 1/W_0$ represents the lifetime in the absence of transfer processes.

Examples of the temporal population evolution of the $^5S_2$ level (under quasi-cw excitation; the pump beam laser is chopped) are presented in Figs. 5(a) and 5(b) for Ho^{3+}:YLF (for two different pump powers and an excitation around 750 nm) and in Figs. 5(c) and 5(d) for Ho^{3+}:$YAlO_3$ (excitation around 754 nm) and Ho^{3+}:BYF (excitation around 888 nm). The experimental setup for such a measurement is close to the emission setup, but in this case the monochromator is fixed to the wavelength at which emission occurs. The signal provided by the photomultiplier is not amplified by a lock-in amplifier and transmitted to the computer, but instead analyzed by an oscilloscope which is operating with the trigger signal from the pumping beam. In order to improve the signal-to-noise ratio, an average over 800–1000 signals was also made with the oscilloscope.

III. DISCUSSION

To start the numerical simulations on a specific system one needs to know the excitation scheme and the parameters involved in the upconversion mechanisms (cross-relaxation rates, pumping rates, phonon deexcitation rates, etc.). The ground-state absorption (GSA), excited-state absorption (ESA), emission, and excitation spectra have to provide the values of the pumping rates and information about the excitation mechanisms, while the lifetime measurements offer information about the values of the cross-relaxation and upconversion rates. The results of the numerical simulations

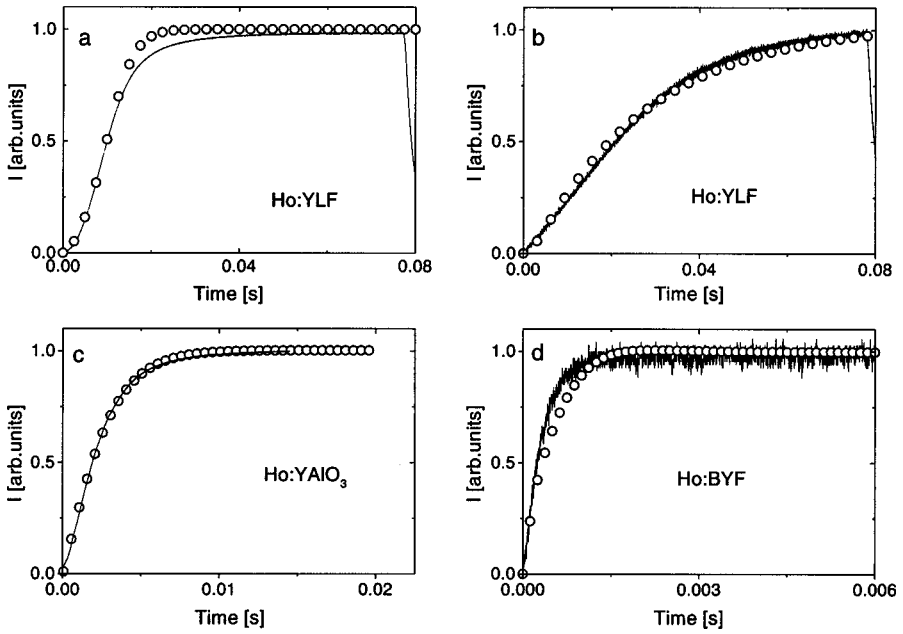

FIG. 5. Temporal evolution of the $^5S_2$ population. The results of the measurements (calculations) are shown as solid lines (open circles). (a) Ho^{3+}:YLF, 750-nm excitation, pumping rate above the threshold. (b) Ho^{3+}:YLF, 750-nm excitation; pumping rate below or around the threshold. (c) Ho^{3+}:$YAlO_3$, 750-nm excitation. (d) Ho^{3+}:BYF, 888-nm excitation.

can be compared with the experimental data of the temporal evolution of the population of the energy level of main interest, i.e., the $^5S_2$ level for the Ho^{3+} ion. Eventually some of the parameters have to be adjusted for a better fit.

Because absorption and emission were already thoroughly studied,[1,3–5,8] we will focus deeper on the ESA and excitation spectra. As we mentioned in Sec. II, in Figs. 2(a)–2(d) the $\Delta I/I$ spectra are presented (dotted line) in comparison with the calculated ESA spectra (determined from the reciprocity method) of the $^5I_7 \leftrightarrow {}^5S_2$ transition for Ho^{3+}:YLF and Ho^{3+}:$YAlO_3$. A good agreement between these two spectra is observed, supporting the conclusion that around 750 nm the main ESA process is the $^5I_7 \rightarrow {}^5S_2$ transition. Nevertheless a second ESA transition, i.e., $^5I_6 \rightarrow {}^5G_6$, occurs in the same wavelength region. A proof for the second ESA process could be the small differences between the two spectra ($\Delta I/I$ and the calculated ESA spectrum) that can be observed especially in the case of Ho^{3+}:$YAlO_3$. However, because of the relatively good agreement between the two spectra we assume that the $^5I_6 \rightarrow {}^5G_6$ ESA process is much weaker than the $^5I_7 \rightarrow {}^5S_2$ ESA process, and accounts only for about 10–15% of the spectrum.

The excitation spectra for the $^5S_2 \rightarrow {}^5I_8$ emission are presented in Figs. 4(a)–4(d) for Ho^{3+}:BYF, Ho^{3+}:YLF, Ho^{3+}:$YAlO_3$, and Ho^{3+}:YSGG in comparison with the $^5I_7 \rightarrow {}^5S_2$ ESA-spectra for Ho^{3+}: YLF (b), Ho^{3+}:$YAlO_3$ (c), and Ho^{3+}:YSGG (d) and in comparison with GSA spectra for Ho^{3+}:BYF (a). A very good agreement in observed for Ho^{3+}:YLF while for Ho^{3+}:$YAlO_3$ and Ho^{3+}:YSGG some differences between the two spectra exist in the relative intensities of the peaks. These differences can be due to the ratio between the two ESA processes at a specific wavelength and/or between the ground-state absorption and the ESA process. These differences support the idea that in the case of Ho^{3+}:YSGG and Ho^{3+}:$YAlO_3$ the second ESA process plays a more important role in populating the $^5S_2$ level than in the case of Ho^{3+}:YLF.

For Ho^{3+}:BYF the ESA spectra are shown in Figs. 3(a) and 3(b). Strong ESA processes exist around 750 and 888 nm (also see Sec. II). The excitation spectra for the green emission for Ho^{3+}:BYF is compared with the ground-state absorption spectra in Fig. 4(a) for the spectral region around 890 nm. Maximal green emission occurs for excitation at about 888 nm, i.e., at a wavelength of a good overlap between GSA and ESA. For the other strong absorption peaks only a weak green emission occurs. This confirms that the main upconversion process is the two-step absorption, as already mentioned in Sec. I.

An estimation of the ratios between the two integral ESA processes ($^5I_7 \rightarrow {}^5S_2$ and $^5I_6 \rightarrow {}^5G_6$ for the case of 750-nm excitation) and between the ESA and GSA processes ($^5I_7 \rightarrow {}^5S_2$ and $^5I_8 \rightarrow {}^5I_4$ for the case of 750-nm excitation and $^5I_5 \rightarrow {}^5F_1$ and $^5I_8 \rightarrow {}^5I_5$ for the case of 888-nm excitation) can be obtained from the Judd-Ofelt theory[14,15] using Eqs. (6) and (7):

$$D(aJ,bJ') = e^2 \sum \Omega_t \langle f^n[\alpha SL]J \| U^t \| f^n[\alpha' S' L']J' \rangle, \tag{6}$$

$$\langle f^n \alpha SLJ \| U^t \| f^n \alpha' S' L' J' \rangle = (-1)^P [(2J+1)(2J'+1)]^{1/2} \begin{Bmatrix} L & t & L' \\ J' & S & J \end{Bmatrix} \times \langle f^n \alpha SL \| U^t \| f^n \alpha' S' L' \rangle, \tag{7}$$

with D the dipol strength, a/b the initial or final state of the transition, J/J' the total quantum moment of the initial or final state of transition, e the elementary charge, Ω_t the Judd-Ofelt parameters ($t=2$, 4, and 6), f^n the denotation of the configuration, L/S the angular-spin moment, $[\alpha LS]J$ the representation of the wave function of the $^{2S+1}L_J$ term in the intermediate coupling scheme, $P=S+L'+t+J$, and $\{{}^{L\ t\ L'}_{J'\ S\ J}\}$ the 6-j symbol. The term $\langle f^n[\alpha SL]J \| U \| f^n[\alpha' S' L']J' \rangle$ represents the double-reduced matrix elements, and can be calculated from Eq. (7), also taking into account the SL states in the intermediate coupling scheme.[16]

We have found that the ratio ESA1/ESA2 [see Fig. 1(a)] is about 5 for Ho^{3+}:$YAlO_3$, 6 for Ho^{3+}:YLF, and 4.5 for Ho^{3+}:YSGG. The estimation of the rate between the ground-state absorption ($^5I_8 \rightarrow {}^5I_4$) and the ESA process ($^5I_7 \rightarrow {}^5S_2$) is also possible; it is about 1/100 for Ho^{3+}-doped YLF, $YAlO_3$, and YSGG. In the case of Ho^{3+}:BYF and excitation at 888 nm, for the integrated ratio GSA2/ESA3 this method gives a result around 0.4. All these values from Judd-Ofelt theory are only approximations, as they represents integral ratios of the transitions between multiplets and not between Stark levels. They were used only for comparison.

In order to obtain the transfer rates, the results of the lifetime measurements were used. For Ho^{3+}:$YAlO_3$ the $^5S_2$ lifetime decreases from 48 μs (0.1% Ho^{3+} doping, 300 K) to effective lifetimes of 33 μs (1% Ho^{3+} doping, 300 K) and 12.7 μs (3% Ho^{3+} doping, 300 K). For Ho:YLF the reduction is from 80 μs (0.5% Ho^{3+} doping, 300 K) to 35 μs (3% Ho^{3+} doping, 300 K). The calculated transfer rates W_t [Eq. 4(a)] are 6.5×10^4 s^{-1} for 3% Ho^{3+}:$YAlO_3$ and 1.6×10^4 s^{-1} for 3% Ho^{3+}:YLF respectively. We have to mention that in the case of $YAlO_3$ under 750-nm excitation a weak blue emission around 390 and 425 nm was observed, corresponding to the transitions $^5G_4 \rightarrow {}^5I_8$ and $^3G_5 \rightarrow {}^5I_8$, respectively. (Note that the $^3G_5$ multiplet also contains terms from the $^5G_5$ multiplet due to the intermediate coupling scheme.) To explain these emissions, the upconversion process σ_1 $[(^5S_2, {}^5S_2) \rightarrow (^5G_4, {}^5I_5)]$ [see Fig. 1(a)] is introduced. For Ho^{3+}:YLF these emissions were not observed.

For a better understanding of the processes, in accordance with the excitation schemes described above we have set a general system of rate equations, see Eqs. (8). Nevertheless for each particular case of excitation scheme there are specific assumptions to be taken into account:

$$\frac{dn_0}{dt} = w_1 {}^* n_1 + \sum_{i=2}^{9} \beta_i {}^* w_i {}^* n_i - R_{11} {}^* n_0 - R_{21} {}^* n_0 - s {}^* n_0 {}^* n_6 - s_2 {}^* n_7 {}^* n_0,$$

TABLE II. Parameter for $Ho^{3+}:YAlO_3$.

Level	$^5I_7$	$^5I_6$	$^5I_5$	$^5I_4$	$^5F_5$	$^5S_2$	$^5F_3$	$^5G_4$
Phonon deexcitation rate w_{i0} (s^{-1})	-	2.4×10^3	2×10^5	-	-	1.7×10^4	-	-
Radiative deexcitation rate w_i (s^{-1})	115	312	260	-	-	4080	-	-
Branching ratio to $^5I_8$	1	0.85	0.4	-	-	0.54	-	-

$$\frac{dn_1}{dt} = -w_1{*}n_1 + w_{20}{*}n_2 + \sum_{i=2}^{9}(1-\beta_i){*}w_i{*}n_i + s{*}n_0{*}n_6 + s_2{*}n_7{*}n_0 - R_{12}{*}n_1,$$

$$\frac{dn_2}{dt} = -w_2{*}n_2 - w_{20}{*}n_2 + w_{30}{*}n_3 - R_{13}{*}n_2,$$

$$\frac{dn_3}{dt} = -w_3{*}n_3 - w_{30}{*}n_3 + w_{40}{*}n_4 + R_{21}{*}n_0 - R_{22}{*}n_3 + s_1{*}n_6{*}n_6,$$

$$\frac{dn_4}{dt} = -w_4{*}n_4 - w_{40}{*}n_4 + w_{50}{*}n_5 + R_{11}{*}n_0 + s{*}n_0{*}n_6,$$

$$\frac{dn_5}{dt} = -w_5{*}n_5 - w_{50}{*}n_5 + w_{60}{*}n_6 + s_2{*}n_7{*}n_0, \qquad (8)$$

$$\frac{dn_6}{dt} = -w_6{*}n_6 - w_{60}{*}n_6 + w_{70}{*}n_7 + R_{12}{*}n_1 - s{*}n_6{*}n_0 - 2{*}s_1{*}n_6{*}n_6,$$

$$\frac{dn_7}{dt} = -w_7{*}n_7 - w_{70}{*}n_7 + w_{80}{*}n_8 - s_2{*}n_7{*}n_0,$$

$$\frac{dn_8}{dt} = -w_8{*}n_8 - w_{80}{*}n_8 + w_{90}{*}n_9 + R_{22}{*}n_3 + R_{13}{*}n_2,$$

$$\frac{dn_9}{dt} = -w_9{*}n_9 - w_{90}{*}n_9 + s_1{*}n_6{*}n_6,$$

$$n = n_0 + n_1 + n_2 + n_3 + n_4 + n_5 + n_6 + n_7 + n_8 + n_9,$$

where n_i (with i from 0 to 9) represents the populations of the $^5I_8$, $^5I_7$, $^5I_6$, $^5I_5$, $^5I_4$, $^5F_5$, ($^5S_2+^5F_4$), $^5F_3$, ($^5G_6+^5F_1$), and $^5G_4$ multiplets, respectively; w_i represents the radiative deexcitation rate for the ith level; w_{i0} denotes the multiphonon deexcitation rate for the ith level; β_i (with i from 2 to 9) are the branching ratios from the ith level to the $^5I_8$ ground state; s is the cross-relaxation rate [($^5S_2$, $^5I_8$) $\rightarrow$($^5I_4$, $^5I_7$)]; s_1 is the upconversion rate [($^5S_2$, $^5S_2$) $\rightarrow$($^5G_4$, $^5I_5$)]; s_2 describes the cross-relaxation [($^5F_3$, $^5I_8$)$\rightarrow$($^5F_5$, $^5I_7$)]; R_{1j} (with j from 1 to 3) represent the pumping rate for the processes $^5I_8\rightarrow{}^5I_4$, $^5I_7\rightarrow{}^5S_2$, and $^5I_6\rightarrow{}^5G_6$, respectively (for the 750-nm pumping scheme); and R_{2k} (with $k=1$ and 2) represents the pumping rates for the process $^5I_8\rightarrow{}^5I_5$ and $^5I_5\rightarrow{}^5F_1$, respectively (for the 888-nm pumping scheme).

The values for phonon deexcitation rates and radiative deexcitation rates were taken from[8,9,17–19] and are listed in the Tables II–IV. The pumping rates were estimated using the well-known formula $R=I{*}\sigma_{abs}/S$, where I is the fluence of the pump (in photons/s), σ_{abs} represents the absorption cross section, and S is the pump beam spot size. The cross-relaxation rates were estimated from the lifetime measurements. The ratios between the pumping rates $R_{11}:R_{12}:R_{13}$ are 1:110:12 for $Ho^{3+}:YAlO_3$ (Ref. 3) and 1:90:11 for Ho^{3+}:YLF. For Ho^{3+}:BYF, the ratio $R_{21}:R_{22}$ is 1:4. In the case of YLF and $YAlO_3$, due to the high phonon energy, we made the assumption that the multiphonon deexcitation is the main process in the deexcitation of the $^5I_4$, $^5I_5$, $^5F_3$, and $^5G_4$ levels (this means, in our case, that all excitations above the $^5S_2$ level end in the $^5S_2$ level and the excitations in the $^5I_4$ and $^5I_5$ levels end in the $^5I_6$ level). For BYF only the phonon deexcitation $^5G_6\rightarrow{}^3K_8\rightarrow{}^5F_2\rightarrow{}^5F_3$ is considered to be stronger than the radiative deexcitation of the $^5G_6$ level. For the calculations, only the cross-relaxation rates (and for Ho^{3+}:BYF also the deexcitation rates) for the $^5G_4$ level were slightly adjusted. The obtained values for the best fit are listed in Table V.

The results from the numerical solution of the system were compared with the experimental results of the temporal evolution of the $^5S_2$ population; see Figs. 5(a)–5(d). Figures 5(a) and 5(b) present the case of Ho^{3+}:YLF for two different

TABLE III. Parameter for Ho^{3+}:YLF.

Level	$^5I_7$	$^5I_6$	$^5I_5$	$^5I_4$	$^5F_5$	$^5S_2$	$^5F_3$	$^5G_4$
Phonon deexcitation rate w_{i0} (s^{-1})	-	350	1.43×10^4	-	3.66×10^4	6.45×10^3	1×10^5	-
Radiative deexcitation rate w_i (s^{-1})	58	125	100	-	1400	2200	2500	-
Branching ratio to $^5I_8$	1	0.92	0.41	-	0.78	0.75	0.53	-

TABLE IV. Parameter for Ho^{3+}:BYF.

Level	$^5I_7$	$^5I_6$	$^5I_5$	$^5I_4$	$^5F_5$	$^5S_2$	$^5F_3$	$^5G_4$
Phonon deexcitation rate w_{i0} (s^{-1})	-	30	2.5×10^4	-	2×10^4	7×10^2	2×10^4	5×10^4
Radiative deexcitation rate w_i (s^{-1})	71	180	51	-	2×10^3	2.7×10^3	2×10^3	10^5
Branching ratio to $^5I_8$	1	0.91	0.41	-	0.78	0.75	0.55	-

pump rates (above and below or around the avalanche threshold value). A threshold value was not observed in the pump power dependence of the green emission.[3] This is probably due to a small value for the pump threshold (thus the experimental error is increased) or/and due the collection of emission signals from different areas of the sample, i.e., areas, where the avalanche regime occurs and areas, where the normal regime occurs.

The results from the numerical simulations are in good agreement with the experimental results for Ho^{3+}:YLF and Ho^{3+}:$YAlO_3$ under 750-nm excitation, and for Ho^{3+}:BYF under 888-nm excitation. However, the reason for the different upconversion behavior for Ho^{3+}:YLF in comparison to Ho^{3+}:$YAlO_3$ is not absolutely clear. As we mentioned in Sec. I we will try an analysis similar to those from Ref. 6, in order to distinguish which part of upconversion mechanism is responsible for the different behaviors of Ho^{3+}:YLF and Ho^{3+}:$YAlO_3$.

We will start by describing in a few words the avalanche process. An avalanche is a specific type of nonlinear upconversion mechanism, based on a strong ESA process originating from an intermediate level usually called ''reservoir level.'' The process starts with a weak ground-state absorption; after that the role of feeding the reservoir level is taken over by a cross-relaxation process. The population of the reservoir level is then strongly increased and hence, because of the strong ESA process, the population of the emitting level. A threshold value for the pumping rate, determined by the ratio between the ESA and GSA cross sections and by the cross-relaxation rate, has to be reached to establish such a process. Characteristics of the process are the specific temporal evolution of population of the emitting level: at pumping rates above the threshold value the shape of the temporal evolution presents a change in the curvature from convex to concave and a specific behavior of the pump power dependence of the emission. Furthermore, around the threshold value of the pump rate the emission is strongly increased. Detailed descriptions of such a process are provided by several authors.[20–22] As it was presented now by both systems, Ho^{3+}:$YAlO_3$ and Ho^{3+}:YLF have the initial conditions (weak GSA, strong ESA, and a cross-relaxation process) for hosting a possible avalanche process. In the case of Ho^{3+}:YLF (Ref. 3) the change of the shape of the temporal population evolution for the $^5S_2$ level was observed [see Fig. 5(a)], while in the case of Ho^{3+}:$YAlO_3$ no such sign of an avalanche was observed.

The method which we will use was extensively described in Ref. 6, but for the sake of simplicity for the reader and to emphasise the differences to our case we describe below the main points of the analysis and the physical meaning of the parameters. The method is based on reducing the real system to an imaginary three-level system (see Fig. 6), in which only the ground state [level (1), corresponding to $^5I_8$], the level which enables the ESA process [level (2), corresponding to $^5I_7$], and the emitting level [level (3) corresponding to $^5S_2$] are represented. The reason for the introduction of this simplified system is to find an analytical relation, which is not possible to find for the real system, because it has too many energy levels involved. This simplified system describes with the help of the parameters of the system (i.e., cross-relaxation rates, pumping rates, and deexcitation rates) the temporal behavior (or at least the tendency of the temporal behavior) of the level populations. With the help of such a relation it is then possible to estimate if an avalanche behavior exists or not. However, even if the number of the levels involved in the calculation will be smaller as in the real system, the parameters that affects the three levels of the simplified system (i.e., cross-relaxation rates, upconversion rates, and excited-state absorption rates) will have to be modified in order to take into account the effects for the other levels.

The fourth level [level (4) in Fig. 6] is necessary to show

TABLE V. Cross-relaxation parameter.

System	$s(^5S_2, {}^5I_8)\rightarrow(^5I_4, {}^5I_7)$ ($s^{-1}cm^{-3}$)	$s_1(^5S_2, {}^5S_2)\rightarrow(^5G_4, {}^5I_5)$ ($s^{-1}cm^{-3}$)	$s_2(^5F_3, {}^5I_8)\rightarrow(^5F_5, {}^5I_7)$ ($s^{-1}cm^{-3}$)
Ho^{3+}:$YAlO_3$ (3%Ho)	0.8×10^{-17}	5.0×10^{-17}	-
Ho^{3+}:YLF 3%(Ho)	3.8×10^{-17}	-	-
Ho^{3+}:BYF (1%Ho)	3.0×10^{-17}	-	4.5×10^{-16}

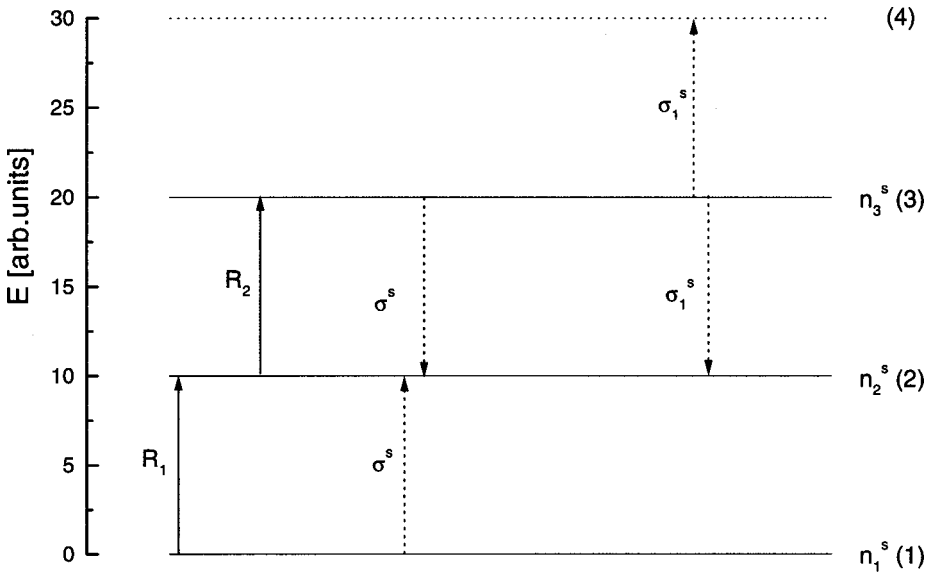

FIG. 6. Simplified model for the description of the upconversion process.

the upconversion process σ_1. It represents all levels lying energetically above the $^5S_2$ multiplet, and will be neglected in the calculations (as above in the numerical simulations). In this simplified system [Eq. (9)] the parameters will be noted as much as possible in the same manner as in the original paper but also taking into consideration the notation from the initial system [Eq. (8)]:

$$\frac{dn_1^s}{dt} = (w_2^s + w_{20}^s)*n_2^s + B*w_3^s*n_3^s - \sigma^{s*}n_1^s*n_3^s - R_1^s*n_1^s,$$

$$\frac{dn_2^s}{dt} = -(w_2^s + w_{20}^s)*n_2^s + (1-B)*w_3^s*n_3^s + w_{30}^s*n_3^s + 2*\sigma^{s*}n_1^s*n_3^s - R_2^s*n_2^s + R_1^s*n_1^s + \sigma_1^s*n_3^s*n_3^s, \tag{9}$$

$$\frac{dn_3^s}{dt} = -w_3^s*n_3^s - w_{30}^s*n_3^s + R_2^s*n_2^s - \sigma^{s*}n_1^s*n_3^s - \sigma_1^s*n_3^s*n_3^s$$

$$n_1^s + n_2^s + n_3^s = 1,$$

where n_1^s, n_2^s, and n_3^s are the populations of the three levels (1), (2), and (3), respectively; R_1^s and R_2^s are the ground- and excited-state absorption pump rates, respectively; σ^s is the cross-relaxation rate $[(3,1)\rightarrow(2,2)]$; σ_1^s is the upconversion rate $[(3,3)\rightarrow(2,4)]$; B is the branching ratio for the radiative deexcitation $(3)\rightarrow(1)$; w_3^s and w_{30}^s are the rates for radiative and phonon deexcitation of level (3), respectively, with $w_3^s + w_{30}^s = 1/\tau_3^s$, where τ_3^s is the effective lifetime of the emitting level in the absence of any cross-relaxation process; and w_2^s and w_{20}^s are the rates for radiative and phonon deexcitation of level (2), respectively, with $w_2^s + w_{20}^s = 1/\tau_2^s$. Because level (2) corresponds to $^5I_7$ and the phonon deexcitation rate for this level is very weak, we will set $w_{20}^s \sim 0$. All these rates (denoted by an upper index s) are characteristic parameters of the simplified model. Our task will be to establish a relation between them and to relate these parameters to those from the real system [Eq. (8)], in order to characterize the possibility of an avalanche mechanism to occur.

In order to study the evolution of the system we will first make the assumption that if we work under low pump rates, the ground state will be almost undepleted, so we can consider $n_1 \sim$ const and close to 1. This assumption also allows us to make the substitution $\sigma_1^{s*}n_3^{s*}n_3^s = \sigma_1^{s*}(1-n_1^s-n_2^s)*n_3^s \approx \sigma_1^{s*}n_3^s(1-n_1^s)$ (the product $n_2^{s*}n_3^s$ is small in comparison to $n_1^{s*}n_3^s$). Then, in accordance with Eq. (5) from Sec. II, we will extend the definition for the quantum yield of a transfer rate to any kind of rate (upconversion, multiphonon deexcitation, etc.). Let us assume that a specific level is affected by deexcitation rates denoted by w_m, w_n, and w_p. In this case the quantum yield of the w_m deexictation process is defined as $w_m/(w_m+w_n+w_p)$. The quantum yield represents the population fraction, which leaves the level due to the process characterized by the rate w_m. In our further calculations we use the following notations for specific quantum yields for the deexcitation processes of level (3) to level (2):

$$H_{CR} = \frac{\sigma^{s*}n_1^s}{\frac{1}{\tau_3^s} + \sigma^{s*}n_1^s + \sigma_1^{s*}(1-n_1^s)}$$

represents the quantum yield of the cross-relaxation process σ^s,

$$H_{UC} = \frac{\sigma_1^{s*}(1-n_1^s)}{\frac{1}{\tau_3^s} + \sigma^{s*}n_1^s + \sigma_1^{s*}(1-n_1^s)}$$

represents the quantum yield of the upconversion process σ_1^s,

$$\eta_1 = \frac{(1-B)*w_3^s}{\frac{1}{\tau_3^s} + \sigma^{s*}n_1^s + \sigma_1^{s*}(1-n_1^s)}$$

represents the quantum yield of the radiative deexcitation, and

$$\eta_2 = \frac{w_{30}^s}{\frac{1}{\tau_3^s} + \sigma^{s*} n_1^s + \sigma_1^{s*}(1-n_1^s)}$$

represents the quantum yield of multiphonon deexcitation. For further simplification we use the notations $H = H_{CR} + H_{UC}$ and $\eta = \eta_1 + \eta_2$

The equation for n_3^s under steady-state condition (i.e., $dn_3^s/dt = 0$) gives the following relation between the populations of levels (2) and (3): $n_3^s = n_2^{s*} R_2^{s*} (1-H)^* \tau_3^s$. With the help of this relations and $n_1^s = 1 - n_2^s - n_3^s$, the rate equation for n_2^s becomes

$$\frac{dn_2^s}{dt} = n_2^{s*} R_2^{s*} (2^* H_{CR} + H_{UC} + \eta - 1) - \frac{1}{\tau_2} - R_1^{s*} R_2^{s*} \tau_3^s (1-H)^* n_2^s - R_1^{s*} n_2^s + R_1^s .$$

Solving this equation, a solution of the type $1/A^*(e^{A^* t} + M)$ is obtained, where t is the time, $M = R_1$, and

$$A = R_2^{s*}(2^* H_{CR} + H_{UC} + \eta - 1) - \frac{1}{\tau_2^s} - R_1^{s*} R_2^{s*} \tau_3^s (1-H) - R_1^s . \quad (10)$$

The behavior of this solution describes what happens with the population of level (2) under a low pump rate and when the population of level (3) is under a steady-state condition. A negative value for A will also provide a steady-state solution for the population of level (2). When A is or becomes positive the population of level (2) has the tendency to increase strongly. Due to the ESA process the increase of the population in level (2) generates an increase of the population in level (3) (which we assumed to be under steady-state conditions). This contradiction means that the system has the tendency to become unstable (regarding to the assumption that we have made). In this case the avalanche mechanism occurs (one of the characteristics of avalanche is that around a threshold value of the pumping rate and/or the cross-relaxation rate, a strong increase in the emission intensity occurs). In conclusion, if A is positive, there is the possibility of an avalanche process occurring. If A is negative, however the system is characterized just by a looping mechanism.

Looking in detail at Eq. (10), we observe that the term $R_2^{s*}(2^* H_{CR} + H_{UC} + \eta - 1)$ represents the gain of the loop, because it can be obtained from the second rate equation of the equation system (9), i.e., from $(1-B)^* w_3^* n_3^s + 2^* \sigma^* n_1^{s*} n_3^s - R_2^* n_2^s$ [this term describes the excitation which returns to level (2) after a pump process R_2^s]. The term $(-1/\tau_2^s) - R_1^{s*} R_2^{s*} \tau_3^s (1-H) - R_1^s$ represents the loss due to radiative deexcitation $(-w_2)$ and due to accumulation of population in the levels (2) and (3). It is obtained by replacing $R_1^{s*} n_1^s$ in the second rate equation of the equation system (9) by $R_1^{s*}(1 - n_2^s - n_3^s)$.

We now have to determine the relations between the parameters of the simplified model $(R_1^s, R_2^s, \sigma^s, \sigma_1^s, w_i^s, w_{0i}^s)$ and the parameters used in the numerical calculations of the real system $(R_1, R_2, \sigma, \sigma_1, w_j, w_{0j})$. In the simplified model the rate R_1^s describes the $1 \rightarrow 2$ transition. These levels [(1) and (2)] correspond to $^5I_8$ and $^5I_7$ in the real system. The ground-state absorption GSA1 (R_1) describes the $^5I_8 \rightarrow {}^5I_4$ transition in the real system. The excitation relaxes from $^5I_4$ to $^5I_7$ by phonon deexcitation ($^5I_4 \rightarrow {}^5I_5 \rightarrow {}^5I_6 \rightarrow {}^5I_7$). This means that we have to take into account the quantum yield of the phonon deexcitation processes for the levels $^5I_4$, $^5I_5$, and $^5I_6$, respectively. In the numerical solution for the real Ho^{3+}:$YAlO_3$ and Ho^{3+}:YLF systems we have assumed that the phonon deexcitation is much larger than the radiative deexcitation for the $^5I_4$ and $^5I_5$ levels, we have $\eta_{40} = \eta_{30} = 1$ and $R_1^s = R_1^* \eta_{20}$. R_2^s describes the $2 \rightarrow 3$ transition in the simplified model. Levels (2) and (3) are levels $^5I_7$ and $^5S_2$ in the real system. The ESA2 process (R_2) describes the transition $^5I_7 \rightarrow {}^5S_2$; thus $R_2^s = R_2$. The cross-relaxation rate σ^s represents the process $(3,1) \rightarrow (2,2)$ in the simplified system. Because of the correspondence $3 \leftrightarrow {}^5S_2$, $2 \leftrightarrow {}^5I_7$, and $1 \leftrightarrow {}^5I_8$, σ^s represents the process $(^5S_2, {}^5I_8) \rightarrow ({}^5I_7, {}^5I_7)$. In the real system the rate s represents the process $(^5S_2, {}^5I_8) \rightarrow ({}^5I_7, {}^5I_4)$. As stated above, the quantum yield of the cross-relaxation process (H_{CR}) represents the percentage from the population of $^5S_2$, which leaves the $^5S_2$ level due to cross-relaxation processes. In the case of the simplified system the excitation removed from $^5S_2$ goes directly to $^5I_7$, while in the real system it ends on the $^5I_4$ level and requires phonon deexcitation processes to end in the $^5I_7$ level. The second component of the cross-relaxation process, i.e., $^5I_8 \rightarrow {}^5I_7$, is identical in the simplified and real systems. Thus we obtain $2^* H_{CR} = \eta_\sigma + \eta_\sigma{}^* \eta_{40}{}^* \eta_{30}{}^* \eta_{20} = \eta_\sigma + \eta_\sigma{}^* \eta_{20}$, where η_σ represents the quantum yield of s. The upconversion rate σ_1^s describes the process $(3,3) \rightarrow (2,4)$, which corresponds to $(^5S_2, {}^5S_2) \rightarrow ({}^5G_4, {}^5I_5)$ in the real system. In the same way as for the cross-relaxation process σ^s we obtain $H_{UC} = \eta_{\sigma_1} + \eta_{\sigma_1}{}^* \eta_{30}{}^* \eta_{20} = \eta_{\sigma_1} + \eta_{\sigma_1}{}^* \eta_{20}$, where η_{σ_1} represents the quantum yield of s_1, i.e., the upconversion process in the real system. A process which exists in the real system is the second ESA process $(R_3, {}^5I_6 \rightarrow {}^5G_6)$. Because this process does not start from the $^5I_7$ level, we cannot include it in the ESA process $2 \rightarrow 3$. Nevertheless this second ESA process populates the $^5S_2$ level in the real system. This means that an additional excitation is brought to the $^5S_2$ level due to R_3. Therefore, we will split the population of the $^5S_2$ level in two components $n_3^{R_2}$ and $n_3^{R_3}$, representing the $^5S_2$ population due to the R_2 and R_3 pumping processes, respectively. Thus far we transferred all rates from the real system to the simplified system setting the ESA1 process $(2 \rightarrow 3)$ to be equal to R_2. This means that by now the population of level (3) in the simplified system is smaller than the population of the $^5S_2$ level in the real system, because of the neglect of $n_3^{R_3}$. Thus in our simplified system by now we have a smaller effect of all processes that affects level (3). Therefore we will replace the cross-relaxation rate σ_1^s by a larger cross-relaxation

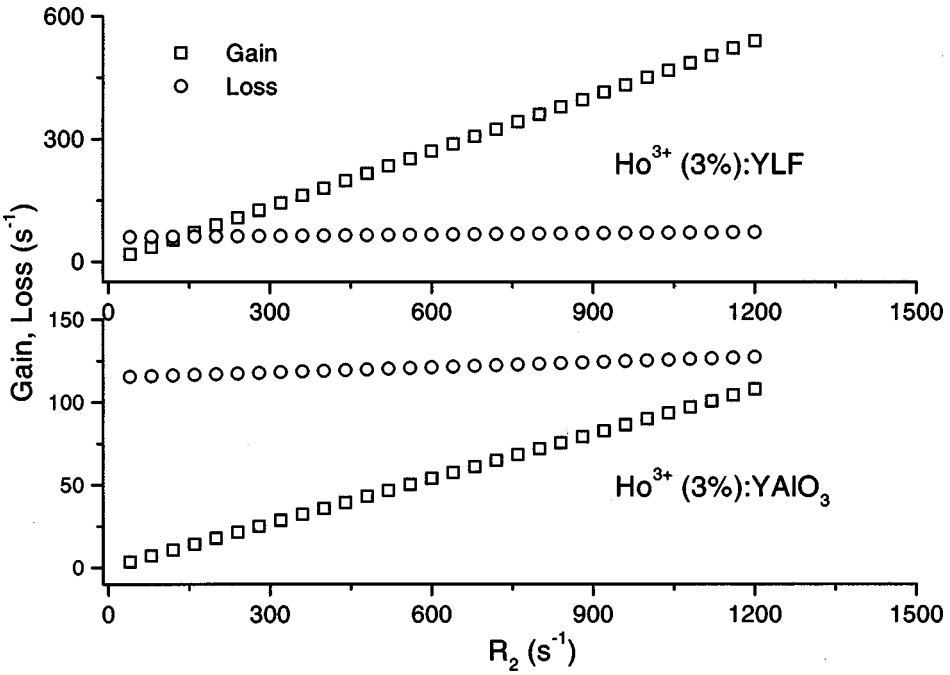

FIG. 7. Gain (open squares) and loss (open circles) for Ho^{3+}:YLF and Ho^{3+}:$YAlO_3$ as a function of the pump rate at 750 nm.

rate σ^s_{NEW} which we will define as follows: $\sigma^s_{\mathrm{NEW}}*(n_3^{R_2}) = (\sigma_1^s+\sigma_X^s)*(n_3^{R_2}) = \sigma_1^s*(n_3^{R_2}+n_3^{R_3})$, with σ^s_{NEW} as the new cross-relaxation rate and σ_X^s as the difference between the new cross-relaxation rate and the old one. This gives

$$\sigma^s_{\mathrm{NEW}} = \sigma_1^s * \left(1 + \frac{n_3^{R_3}}{n_3^{R_2}}\right). \tag{11}$$

The same calculation can be made for the other rates that affect the $^5S_2$ population (i.e., the phonon deexcitation rate, the upconversion rate, and the radiative deexcitation rate). In the simplified system we therefore have to increase [as in Eq. (11)] any of the rates of the processes which start from $^5S_2$ in order to take into account the effect of the $^5I_6 \rightarrow {}^5G_6$ excited-state absorption. An estimation of the ratio $n_3^{R_3}/n_3^{R_2}$ is possible from the numerical evaluation of the real system [Eq. (8)] in the presence and absence of the ESA2 process, i.e., the whole system is solved with the complete set of parameters for $R_3 \neq 0$ and for $R_3 = 0$, respectively. The ratio of the two populations of the $^5S_2$ level obtained in this way will be used to replace $n_3^{R_3}/n_3^{R_2}$. The obtained ratios are about 0.3 for Ho^{3+}:$YAlO_3$ and ~ 0 for Ho^{3+}:YLF. In order to calculate the gain (G) and loss (L) of the whole loop we will put Eq. (10) in the forms

$$G = R_2^s * (2 * H_{\mathrm{CR}} + H_{\mathrm{UC}} + \eta - 1) \tag{12}$$

$$L = \frac{1}{\tau_2^s} + R_1^s * R_2^s * R_1^s * \tau_3^s (1 - H) + R_1^s . \tag{13}$$

With the known relation between the parameters in these two equations and the real parameters of the Ho^{3+}:YLF and Ho^{3+}:$YAlO_3$ systems, we are now able to calculate the gain and loss. In Fig. 7 the gain and loss for $Ho^{3+}(3\%)$:$YAlO_3$ and $Ho^{3+}(3\%)$:YLF are shown. For a pumping rate of about 1.1×10^3 s^{-1} (which corresponds to a pump power of about 1.8–1.9 W for a circular pump spot of 100μm diameter) in the $Ho^{3+}(3\%)$:$YAlO_3$ system the gain is about 100–110 s^{-1} while the loss is about 130 s^{-1}. Thus A is negative, and a photon avalanche does not occur up to this pumping rate. For the same pumping rate, in $Ho^{3+}(3\%)$:YLF the gain is about 460 s^{-1}, while the loss is only about 80–90 s^{-1}, i.e., the system is in the avalanche regime. This system will reach the photon-avalanche regime at a pumping rate of about 160 s^{-1}.

The reason for this different behavior can be explained with the cross-relaxation rates (listed in Table V) for Ho^{3+}:$YAlO_3$ and Ho^{3+}:YLF. For Ho^{3+}:$YAlO_3$ the $^5I_7$ level is fed mainly by multiphonon deexcitation processes, whereas the cross-relaxation rate s (corresponding to σ^s in the simplified system) is small (quantum yield $\eta_\sigma = 0.09$). In contrast, for Ho^{3+}:YLF the cross-relaxation rate is larger (quantum yield $\eta_\sigma = 0.47$). The case of Ho^{3+}:YSGG will not be further discussed, because the features are very similar to those of Ho^{3+}:$YAlO_3$.

For Ho^{3+}:BYF under 750- and 888-nm excitations, a corresponding analysis is very difficult, because the phonon deexcitation rates are much smaller than in the case of Ho^{3+}:YLF and Ho^{3+}:$YAlO_3$. The assumption that all excitation above the $^5S_2$ level ends via phonon deexcitation in the $^5S_2$ level (as used for Ho^{3+}:YLF and Ho^{3+}:$YAlO_3$) is not valid in this case. The reduced model becomes too complicated, because the necessary introduction of additional levels makes it nearly impossible to estimate the relation between the parameters of the real system and the simplified system. It should also be noted, that in the case of 888-nm excitation there is no cross-relaxation process feeding the $^5I_5$ intermediate level. Thus the gain of a hypothetical loop starting from this level will be based only on phonon deexcitation and therefore small. In the same time the loss term in the

TABLE VI. Inversion pump rates R_1 and pump powers P_1 for the systems investigated under different pump wavelengths λ_p for obtaining the inversion between the lowest Stark level of the combined ($^5S_2$, $^5F_4$) multiplet and the highest Stark level of the $^5I_8$ ground state. $n(Ho^{3+})$: Ho^{3+} concentration in the crystal. A pump spot diameter of 100 μm was assumed in the calculations.

System	$n(Ho^{3+})$	λ_p (nm)	R_1 (s^{-1})	P_1 (W)	Comments
Ho^{3+}:YLF	3%	750	9×10^3	~16	
Ho^{3+}:$YAlO_3$	3%	750	2×10^4	~35	At $R_2=9\times10^3$ the ratio between the lowest Stark level of the $^5S_2$ level and the highest Stark level of $^5I_8$ is 0.4.
Ho^{3+}:BYF	1%	888	4.6×10^3	~18	
Ho^{3+}:$YAlO_3$	1%	750	2.7×10^4	~50	At $R_2=4.6\times10^3$ the ratio between the lowest Stark level of the $^5S_2$ level and the highest Stark level of $^5I_8$ is 0.1.

loop, i.e., $R_1^s * R_2^s * \tau_3^s (1-H)$ is high due to the high ground-state absorption rate. Furthermore, the ground-state absorption cannot be considered as weak, and therefore a rapid, significant change in the population of the ground state will occur, which is a contradiction to the assumption of an undepleted ground state.

With the help of Eqs. (8) an estimation of the efficiency of the whole upconversion process with respect to the realisation of laser oscillation is possible. Therefore, the necessary pump rate for obtaining population inversion between the lowest Stark level of the thermally coupled ($^5S_2$, $^5F_4$) multiplets and the highest Stark level of the $^5I_8$ ground state is calculated and denoted by R_I (corresponding to the ESA1 process for 750-nm pumping or to the ESA3 process for 888-nm pumping). The results under the assumption of a pump spot diameter of 100 μm are listed in Table VI. It can be seen that pump powers of 16–18 W are at least necessary to reach threshold inversion. Therefore, in the cases of infrared excitation in the range of 700–900 nm, the singly Ho^{3+}-doped systems investigated by us are not very promising for a realization of laser oscillation on the green transition. The above calculations were performed in a constant pump rate model, i.e., the numerical system does not take into account the spatial distribution of the pump. However, for the cases of 750-nm pumping, codoping with other rare-earth ions should be taken into consideration in order to improve the transfer rates and thus to lower the inversion pump rate. In case of Yb^{3+} codoping a significant improvement in the emission intensity and efficiency of the upconversion process was observed[23] and further investigation in this direction are under way.

IV. CONCLUSION

The Ho^{3+}-ion was investigated in some crystalline hosts under excitation in the spectral range between 700 and 920 nm. Excited-state absorption processes occurring from the $^5I_7$, $^5I_6$, and $^5I_5$ levels were spectroscopically investigated. A characteristic feature of Ho^{3+}-doped systems is the occurrence of two simultaneous ESA processes ($^5I_7 \rightarrow {}^5S_2$ and $^5I_6 \rightarrow {}^5G_6$) at the same wavelength around 750 nm. The ratio between these two ESA processes seems to be similar for the crystals studied although the influence of the second ESA process is important for the population of the $^5S_2$ level in Ho^{3+}:$YAlO_3$ and Ho^{3+}:YSGG, but plays a smaller role in Ho^{3+}:YLF ($n_3^{R_3}/n_3^{R_2}=0.3$ for $YAlO_3$ and 0 for YLF). This difference in the effect of the second ESA process is related to the value of the phonon deexcitation rate and to the value of the cross-relaxation rate: on the one hand, a high phonon deexcitation rate favors that the excitation into the $^5I_5$ and $^5I_6$ levels relaxes into the $^5I_7$ level and the excitation into the $^5F_3$ level relaxes into the $^5S_2$ level; however, on the other hand, a multiphonon quenching of the $^5S_2$ emitting level is also favored. For small multiphonon rates a long lifetime of the emitting level exists, but the $^5I_6$ level acts as a trap for the excitation and also radiative and nonradiative deexcitation via cross-relaxation from the levels above the $^5S_2$ level probably overpass the $^5S_2$ level. A high cross-relaxation rate favors the feeding of the $^5I_7$ level but also depletes strongly the $^5S_2$ level.

In conclusion, we can say that the singly Ho^{3+}-doped systems investigated by us are not promising for the realization of upconversion laser oscillation in the green spectral range ($^5S_2 \rightarrow {}^5I_8$) under and infrared pump in the spectral range between 700 and 900 nm. Nevertheless a host material with a more efficient cross relaxation process ($^5S_2$, $^5I_8$) $\rightarrow$($^5I_7$, $^5I_4$) and/or a more efficient ESA process ($^5I_7 \rightarrow {}^5S_2$) could prove itself to be very suitable for such a purpose. We also proved that the different behavior of the upconverted emission between Ho^{3+}:YLF and Ho^{3+}:$YAlO_3$ is due to the different values of the cross-relaxation rate. This suggests that in the case of Ho^{3+}:$YAlO_3$ a codoping with another ion, e.g., Yb^{3+}, leads to an avalanche mechanism due to higher cross-relaxation rates (in order to efficiently feed the $^5I_6$ and $^5I_7$ levels).[23] Therefore, lower pump rates for reaching threshold inversion are also expected for codoped Yb^{3+}, Ho^{3+}:$YAlO_3$ and Yb^{3+}, Ho^{3+}:YLF systems.

ACKNOWLEDGMENTS

This study was supported by the German DFG Project: KU1158/4-1 and by Polish KBN Project No. 8T11B 08117 in collaboration with DFG Graduiertenkolleg No. 463 at the University of Hamburg.

*Electronic address: osiac@physnet.uni-hamburg.de; FAX: 49 40 42838 6281

[1] M. Malinowski, R. Piramidowicz, Z. Frukacz, G. Chadeyron, R. Mahiou, and M. F. Joubert, Opt. Mater. **12**, 409 (1999).
[2] G. K. Liu, Y. H. Chen, and J. V. Beitz, J. Lumin. **81**, 7 (1999).
[3] S. Kück and I. Sokólska, Chem. Phys. Lett. **325**, 257 (2000).
[4] E. Osiac, J. Alloys Compd. (to be published).
[5] E. Osiac, I. Sokólska, and S. Kück, J. Alloys Compd. **323–324**, 283 (2001).
[6] A. Brenier, L. C. Courrol, C. Pedrini, C. Madej, and G. Boulon, Opt. Mater. **3**, 25 (1994).
[7] J. Koetke and G. Huber, Appl. Phys. B: Lasers Opt. **61**, 151 (1995).
[8] A. M. Tkachuk, A. V. Khilko, and M. V. Petrov, Opt. Spektrosk. **58**, 91 (1985) [Opt. Spectrosc. **58**, 55 (1985)].
[9] Sh. N. Gifeisman, A. M. Tkachuk, V. V. Prizmak, Opt. Spektrosk. **44**, 120 (1978) [Opt. Spectrosc. **44**, 68 (1978)].
[10] A. A. Kaminskii, *Laser Crystals*, 2nd ed. Springer-Verlag, Berlin 1990), p. 140.
[11] J. B. Gruber, M. E. Hills, M. D. Seltzer, S. B. Stevens, and C. A. Morrison, J. Appl. Phys. **72**, 5253 (1992).
[12] V. J. Pugh, F. S. Richardson, J. B. Gruber, and M. D. Seltzer, J. Phys. Chem. Solids **58**, 85 (1997).
[13] A. I. Burshtein, J. Lumin. **34**, 167 (1985).
[14] B. R. Judd, Phys. Rev. **157**, 262 (1962).
[15] G. S. Ofelt, J. Chem. Phys. **37**, 511 (1962).
[16] C. W. Nielson and G. F. Koster, *Spectroscopic Coefficients for the p^n, d^n, f^n Configurations* (MIT Press, Cambridge, MA 1963).
[17] M. J. Weber, B. H. Mastinger, V. L. Donlan, and G. T. Surrat, J. Chem. Phys. **57**, 562 (1972).
[18] A. M. Tkachuk, S. I. Klokishner, A. V. Poletimova, L. M. Mogileva, and M. V. Petrov, Opt. Spektrosk. **60**, 1201 (1986) [Opt. Spectrosc. **60**, 745 (1986)].
[19] B. M. Antipenko, Opt. Spektrosk. **56**, 72 (1984) [Opt. Spectrosc. **56**, 44 (1984)].
[20] R. Scheps, Prog. Quantum Electron. **20**, 4 (1996).
[21] S. Guy, M. F. Joubert, and B. Jacquier, Phys. Rev. B **55**, 8240 (1997).
[22] M. F. Joubert, S. Guy, and B. Jacquier, Phys. Rev. B **48**, 10 031 (1993).
[23] E. Osiac, I. Sokólska, and S. Kück, J. Lumin. **94–95**, 289 (2001).